JNeurosci
THE JOURNAL OF NEUROSCIENCE

Research Articles | Development/Plasticity/Repair

The developmental emergence of tonic and phasic REM sleep in rats

https://doi.org/10.1523/JNEUROSCI.2176-25.2026

Received: 26 November 2025
Revised: 9 March 2026
Accepted: 12 March 2026

The developmental emergence of tonic and phasic REM sleep in rats

John P. Kobrossi[1] and James C. Dooley[1,2†‡]

[1]Department of Biological Sciences, Purdue University, West Lafayette, Indiana
[2]Purdue Institute for Integrative Neuroscience,
Purdue University, West Lafayette, Indiana

[†]Corresponding author: James C. Dooley, Ph.D. (jcdooley@purdue.edu)
[‡]Lead Contact: James C. Dooley

Keywords: neurodevelopment, cortical development, sleep ontogeny, sleep architecture, local field potentials

Abbreviated title: Tonic and phasic REM development

Number of pages: 26

Number of figures: 6, plus 3 supplementary figures

Number of words (abstract): 225

Number of words (introduction): 611

Number of words (discussion): 1478

Conflict of interest statement: The authors declare no competing interests.

Acknowledgments: We thank Mark Blumberg, Greta Sokoloff, Nick Sattler and Madi Reid for feedback on earlier versions of this manuscript. This research was supported by the Sleep Research Society Foundation's Career Development Award to J.C.D. Large language models (i.e. ChatGPT, Google Gemini) were used to revise individual sentences, however no material was written by these models *de novo*.

Author contributions: J.C.D. designed research; J.C.D. performed research; J.C.D. data curation; J.P.K and J.C.D. analyzed data; J.P.K and J.C.D. visualization; J.C.D writing – original draft; J.P.K and J.C.D. writing – review & editing; J.C.D. supervision; J.C.D. resources

Abstract

REM sleep is composed of two substates—phasic and tonic—that differ in their behavioral, sensory, and electrophysiological features. Although these substates are well characterized in

adults, their developmental trajectory remains unclear. Here, we examined the development of tonic and phasic REM in rats of either sex from postnatal day (P) 12–24, spanning a period of rapid corticothalamic development. We recorded local field potentials and single units from primary motor cortex (M1), together with high-speed video and electromyographic recordings of the nuchal muscle. Periods of behavioral quiescence along with high delta power indicated NREM sleep, whereas periods of sustained muscle atonia and low delta power indicated REM sleep. At P16, M1 theta oscillations first appeared, and the delay to the first twitch increased, revealing the start of a distinct twitch-free portion of REM sleep. Motivated by this, we divided REM sleep into phasic and tonic periods, with and without twitching, respectively. Spiking activity and gamma power were consistently higher during phasic REM. At P20, phasic REM also showed faster theta oscillations than tonic REM. At P24, tonic REM was accompanied by a distinct alpha oscillation. These results show that the features distinguishing the two REM substates appear sequentially across development, revealing a progressive differentiation of REM sleep into tonic and phasic periods, a developmental refinement that may support increasingly complex forms of sleep-dependent plasticity.

Significance Statement

Infancy is marked by rapid circuit formation and by the dominance of REM sleep, a state thought to support early neural development. Yet sleep itself undergoes massive changes throughout this period, and the developmental timeline of REM sleep remains poorly understood. Using neural recordings and high-speed video from developing infant rats, we show that REM sleep gradually divides into two substates—tonic and phasic—across infancy. These substates exhibit age-dependent differences in movement, neural firing, and cortical oscillations, revealing increasing microstructural complexity in REM sleep. Our findings identify when these substates first emerge and how their defining features unfold over time, providing a framework for understanding how REM sleep supports developmental plasticity throughout early life.

Introduction

Since its discovery in humans, rapid eye movement (REM) sleep has been described as a paradoxical state, combining wake-like brain activity with sleep-like behavior. This paradox becomes more striking when examining human REM sleep at finer resolution. In adults, REM sleep alternates between phasic and tonic periods, each marked by distinct patterns of movement, cortical activity, and sensory responsiveness (Ermis et al., 2010; Simor et al., 2017, 2020). Phasic REM features bursts of eye movements and muscle twitches against a background of atonia and is accompanied by elevated gamma power and high arousal thresholds (Datta and O'Malley, 2013). Tonic REM, by contrast, is defined by behavioral quiescence, stronger alpha/beta activity, and lower arousal thresholds (Waterman et al., 1993; Wehrle et al., 2007). Despite growing appreciation of this microarchitecture, remarkably little is known about when in development these distinct REM substates first emerge.

In early postnatal life, research in humans and rodents alike shows that the majority of time is spent in REM sleep, also called active sleep in infancy (Jouvet-Mounier et al., 1969; Knoop et al., 2021). Throughout infancy, work in rodents demonstrates that the twitches of REM sleep drive sensory feedback in the developing nervous system (Khazipov et al., 2004; Sokoloff et al., 2015; Dooley and Blumberg, 2018; Dooley et al., 2020). These twitches are abundant at birth, but decline sharply over the first few postnatal weeks (Blumberg et al., 2005; Reid et al., 2025). During this same developmental window, thalamocortical networks undergo rapid development: delta rhythms are established during NREM sleep (Seelke and Blumberg, 2008), sensory responses become more temporally precise (Dooley and Blumberg, 2018; Dooley et al., 2021), and theta oscillations emerge in the brainstem and hippocampus (Del Rio-Bermudez et al., 2017; Muessig et al., 2019). Thus, in rodents, late infancy (P12–P24) represents a window in which REM sleep physiology and cortical function are in continuous flux.

Tonic and phasic REM have been described in adult rodents (Brankačk et al., 2012; Meng et al., 2021; Dong et al., 2022; Bueno-Junior et al., 2023), with each substate sharing many of the features described in humans (see **Table 1**). Although prior research has described age-related changes in the proportion of tonic and phasic REM sleep across development (Vogel et al., 2000), this work did not explore whether there are differences in cortical oscillations or neural activity across age. Consequently, it remains unclear whether these substates emerge fully formed or whether their constituent features develop gradually. Characterizing this developmental progression is essential for linking the well-characterized behavioral and electrophysiological features of REM sleep in infancy to the microarchitecture of REM sleep in adults.

Here, we recorded local field potentials and unit activity from the forelimb region of primary motor cortex (M1) in unanesthetized, head-fixed P12–P24 rats. Behavioral states were characterized via continuous monitoring of nuchal EMG and high-speed video. REM-sleep-associated theta oscillations first appeared in M1 at P16. At the same time, the interval from REM onset to the first twitch lengthened, revealing sustained periods of REM sleep without twitches. Phasic REM consistently showed stronger gamma power and increased neural activity, but across P16 and P24, additional components developed that further differentiated REM sleep into tonic and phasic substates. By P20, theta oscillations during phasic REM were significantly faster than tonic REM, and the duration of tonic REM bouts increased. At P24, tonic REM was also accompanied by a distinct fast-alpha oscillation. Notably, the rate of twitches remained stable within phasic bouts across ages, even as the overall number of twitches declined. Thus, REM sleep continues to develop across infancy—from an early, largely undifferentiated state to one composed of tonic and phasic substates, each with distinct oscillatory signatures.

Materials and Methods

Experimental model and subject details

For this experiment, we performed acute, cross-sectional recordings of neural activity from the primary motor cortex (M1) in Sprague–Dawley rats (*Rattus norvegicus*) in four age groups: postnatal day (P) 12 (N = 9 pups; 30.5 ± 1.9 g; 3 male), P15–16 (hereafter referred to as P16; N = 11 pups; 43.8 ± 3.1 g; 8 male), P18–20 (P20; N = 12 pups; 56.1 ± 4.4 g; 7 male), and P22–24 (P24; N = 10 pups; 68.9 ± 4.4 g; 6 male). Each age cohort consisted of distinct animals, and all pups from an age cohort were from separate litters. Although this study centers on M1 activity, recordings were obtained from the forelimb representation of M1 in combination with either the ventrolateral or ventroposterior nucleus of the thalamus. A subset of these animals has been included in prior studies that characterize their movement-related activity (see Dooley et al., 2021; Reid et al., 2025).

Pups were reared with their dam in standard laboratory cages (48 × 20 × 26 cm) maintained under controlled temperature and humidity on a 12:12 h light–dark cycle, with unrestricted access to food and water. The day of birth was designated P0, and litters were reduced to eight pups by P3. Each pup had at least four littermates until P12 and a minimum of two littermates on the day of recording. Animals remained with the dam until testing, and no pups were weaned before data collection. All procedures followed the National Institutes of Health *Guide for the Care and Use of Laboratory Animals* (NIH Publication No. 80–23) and were approved by the Institutional Animal Care and Use Committees of the University of Iowa and Purdue University.

Method Details

Surgery. A pup of appropriate body weight and, for P12 animals, with a visible milk band was selected from the litter and anesthetized using isoflurane (3–5%; Phoenix Pharmaceuticals, Burlingame, CA). After shaving the scalp, care was taken to preserve all vibrissae. To monitor behavioral state, pairs of custom bipolar hook electrodes (0.002-inch diameter, epoxy-coated wire; California Fine Wire, Grover Beach, CA) were implanted into the nuchal and contralateral biceps muscles. Carprofen (5 mg/kg, subcutaneous; Putney, Portland, ME) was administered for postoperative analgesia.

The scalp was then excised, and a topical anesthetic (bupivacaine; Pfizer, New York, NY) was applied to the exposed skull. After cleaning and drying the skull surface with a mild bleach solution, small areas of residual bleeding were cauterized as needed in P20 and P24 pups to ensure complete dryness of the skull prior to headplate attachment. The surrounding skin was sealed with Vetbond (3M, Minneapolis, MN), and a custom stainless-steel headplate (Neurotar, Helsinki, Finland) was affixed to the skull using cyanoacrylate adhesive.

A 1.8-mm trephine drill (Fine Science Tools, Foster City, CA) was used to open a craniotomy above the forelimb area of M1 (0.5 mm anterior, 2.2–2.5 mm lateral to bregma). When additional recordings were made, a second craniotomy was placed above the thalamus (2.0–2.8 mm caudal to bregma, 2.2–2.5 mm lateral) as described previously (Dooley et al., 2021).

Following surgery, pups were positioned in a custom head-fixation frame mounted to a Mobile HomeCage (NTR000289-01; Neurotar, Helsinki, Finland). This is an air table with a moving platform where the head-fixed pup rests. When the pup attempts to locomote, the enclosure moves around the pup, providing the illusion of movement while the pup's head remains stationary. The height of the head above the cage floor was adjusted according to age such that the body rested naturally on the elbows during REM-related atonia (P12: 35 mm; P16: 38 mm; P20–P24: 40 mm). EMG leads were secured along the back to prevent tangling. Pups recovered

from anesthesia within 15 minutes and were allowed 1–2.5 hours to acclimate to the head-fixation apparatus. This period allowed both electrode stabilization and the reestablishment of normal neural activity (Domínguez et al., 2021). Recording commenced once both one hour had passed and animals displayed characteristic sleep–wake behaviors (**Figure S1**), including twitching, grooming, and spontaneous locomotion.

Recording Environment. Recordings took place inside a sound-attenuating Faraday cage illuminated with constant, flicker-free red light (630 nm; Waveform Lighting, Vancouver, WA). A continuous broadband noise (70 dB) was played throughout the session to mask environmental sounds. To promote extended periods of REM sleep, ambient temperature was maintained between 26.5 °C and 29 °C (Szymusiak and Satinoff, 1981). The pup's head was oriented away from the room entrance to minimize visual disturbance. All monitoring and data collection were performed remotely, with the experimenter positioned outside the room to reduce environmental disruptions and maintain a calm recording environment for the animal.

Electrophysiological Recordings. Nuchal and biceps EMG leads were connected to the analog inputs of a Lab Rat LR-10 system (Tucker-Davis Technologies, Gainesville, FL). EMG signals were amplified, digitized at ~1.5 kHz, and high-pass filtered at 300 Hz.

Prior to implantation, 16-channel silicon depth electrodes (A1x16-3mm-100-177-A16) were coated with the fluorescent tracer DiI (Vybrant DiI Cell-Labeling Solution; Life Technologies, Grand Island, NY). Electrodes were lowered into the forelimb representation of M1 using a multiprobe micromanipulator (New Scale Technologies, Victor, NY) operated via an Xbox controller (Microsoft, Redmond, WA). The array was advanced until all sites were located beneath the dura, typically at a depth of ~1500 µm. A chlorinated Ag/Ag-Cl wire (0.25 mm diameter; Medwire, Mt. Vernon, NY) inserted into the contralateral occipital cortex served as the common reference and ground. Neural activity was digitized at ~25 kHz with a 0.1 Hz high-pass filter to reduce signal drift and notch filters at 60, 120, and 180 Hz.

Recordings were collected continuously for 3–6 hours using SynapseLite software (Tucker-Davis Technologies). The Mobile HomeCage system allowed stable head fixation while permitting natural behaviors—including locomotion, grooming, and sleep—throughout the session. This system utilizes a lightweight carbon-fiber platform that floats on a cushion of air; as the head-fixed animal moves its paws, it propels the floating enclosure around itself. This design accommodates sleep, locomotion, and postural adjustments without the instability associated with tethered, freely-moving preparations.

Video Collection and Synchronization. Video recordings were temporally aligned with the electrophysiological data to permit quantification of movement and behavioral state, as described previously (Dooley et al., 2020). Each pup was enclosed within a transparent chamber positioned inside the Mobile HomeCage, allowing full visual access during recording. A single Blackfly-S camera (FLIR Integrated Systems, Wilsonville, OR) was mounted at a 45° angle relative to the animal's head, centered on the right forelimb contralateral to the cortical recording site. This setup provided a clear view of the right whiskers, forelimb, hindlimb, and tail. Video was captured in SpinView (FLIR Integrated Systems) at 100 frames per second, with a 7-ms exposure time and a resolution of 720 × 540 pixels.

To synchronize video and electrophysiological recordings, a red LED positioned within the camera's field of view was driven by SynapseLite (Tucker-Davis Technologies) to emit a 100-ms pulse every 3 seconds. The timing of these flashes served as a reference signal for frame alignment. Custom MATLAB scripts quantified the number of frames between successive LED pulses to verify recording stability and detect dropped frames. In the rare event that the expected interval (300 frames, corresponding to the 3-s period at 100 frames/s) was not met, a placeholder

frame was inserted at the missing location. This procedure maintained frame-by-frame correspondence between the video and electrophysiological data, ensuring synchronization accuracy within one frame (10 ms) across the entire recording session.

Histology. Following completion of the recording session, pups were deeply anesthetized with ketamine/xylazine (10:1; >0.08 mg/kg) and transcardially perfused with 0.1 M phosphate-buffered saline (PBS), followed by 4% paraformaldehyde (PFA). Brains were removed, post-fixed in 4% PFA for at least 24 hours, and then transferred to a 30% sucrose solution for a minimum of 24 hours prior to sectioning.

To verify electrode placement within the M1 forelimb representation, cortices were sectioned either tangentially to the pial surface or in the coronal plane. For tangential preparations, the right hemisphere was carefully separated from the underlying subcortical tissue and flattened between two glass slides spaced 1.5 mm apart for 5–15 minutes, with light pressure applied using 10 g weights. All brains were cut at a thickness of 80 µm. Wet-mounted sections were imaged under a fluorescent microscope (Leica Microsystems, Buffalo Grove, IL) at 2.5x magnification to visualize DiI fluorescence and confirm electrode tract locations.

Cortical tissue was stained for cytochrome oxidase (CO) to delineate primary cortical areas, which are well defined by this method during the developmental period studied (Seelke et al., 2012). The staining solution consisted of cytochrome C (3 mg/10 mL; Sigma-Aldrich), catalase (2 mg/10 mL; Sigma-Aldrich), and 3,3′-diaminobenzidine tetrahydrochloride (DAB; 5 mg/10 mL; Spectrum, Henderson, NV) dissolved in equal parts phosphate buffer and distilled water. Sections were incubated on a shaker at 35–40 °C (approximately 100 rpm) until the tissue was well differentiated (approximately 3-6 hours), then rinsed in PBS, mounted on glass slides, and air-dried for at least 48 hours. Once dry, slides were cleared in citrus clearing solvent (Richard-Allan Scientific) and cover-slipped with DPX.

Final images were collected at 2.5x or 5x magnification. When needed, multiple images were stitched into a single composite using Microsoft Image Composite Editor (Microsoft, Redmond, WA), allowing electrode tracks to be visualized relative to areal and laminar boundaries of cortex.

Local Field Potential. For analysis of local field potentials (LFP), raw neural signals were first smoothed with a Gaussian moving kernel (half-width: 0.5 ms) to reduce high-frequency noise and then resampled to approximately 1 kHz.

For each recording, one channel was selected for LFP analyses using the following procedure. Channels exhibiting excessive noise or poor correlation with neighboring sites were first excluded. For the remaining channels, a zero-phase digital bandpass filter was applied to isolate delta (0.5–4 Hz) frequency bands. A trained scorer then identified at least five NREM sleep epochs, each lasting a minimum of 10 seconds. The channel displaying the highest delta power during these NREM segments was chosen for all subsequent LFP analyses. This approach typically selected more superficial cortical sites (at a depth of 200-400 µm), as delta power generally declined with depth along the electrode shank. In contrast, theta activity during REM sleep was generally uniform across channels and cortical layers.

ROI Movement Classification. To quantify movement events, frame-by-frame changes in pixel intensity were analyzed within predefined regions of interest (ROIs) using custom MATLAB scripts (Dooley et al., 2021). Unlike markerless tracking algorithms (e.g., DeepLabCut), which are designed to extract precise kinematic features from specific anatomical landmarks, our primary objective was to detect the occurrence of movements, rather than their kinematic trajectory. Consequently, we employed a pixel-difference approach that captures motion within a ROI. This

method is particularly sensitive to the low-amplitude movements characteristic of myoclonic twitches, which may not result in significant translation of tracking key points.

For each ROI, the number of pixels exhibiting an intensity change greater than 5% between consecutive frames was summed, yielding a continuous 100 Hz signal reflecting movement-related pixel variation. This automated detection procedure served as a high-sensitivity screen to identify candidate movements. Because we prioritized minimizing false negatives, thus missing small twitches, we relied on visual inspection of synchronized video recordings to confirm both the occurrence of movement and the specific body part involved. This hybrid approach—sensitive automated detection followed by human verification—ensured accurate differentiation between twitches and other sources of movement like respiration or heart rate, a contextual distinction that remains challenging for purely automated systems.

For twitch analysis, the ROI corresponding to the relevant body part (e.g., forelimb) was examined in Spike2 (Version 8; Cambridge Electronic Design, Cambridge, UK) alongside the video. Peaks in the ROI-derived time series were validated as discrete twitches. Twitch onset was defined as the first frame in which movement activity was detected. For the limbs and tail, this approach reliably captured every visible twitch, as even closely spaced events exhibited distinct onsets and offsets. In contrast, whisker movements sometimes consisted of rapid alternating protractions and retractions without clear boundaries, in which case only the first twitch in a series was counted.

Wake movements were assessed using a ROI encompassing the entire animal because body-part-specific ROIs were less reliable given the variability in limb position during wakefulness. Only wake movements involving the forelimb were included in subsequent analyses. The onset of each wake movement was defined as the first frame in which the forelimb moved independently. To ensure that labeled wake events represented distinct transitions from inactivity to movement, only the initial movement in a bout was marked, and additional movements were annotated only if separated by at least 500 ms of behavioral quiescence.

Classification of Behavioral State. Behavioral state was classified based on concurrent analysis of cortical delta activity and nuchal EMG. For each pup, the rectified EMG signal was dichotomized into periods of high muscle tone and atonia. Five representative segments of each condition were selected (at least 10 seconds in duration), and their median amplitudes were computed. The midpoint between these two medians served as the threshold for distinguishing tone from atonia. Using a running 1-s mean of the rectified EMG, values exceeding this threshold were classified as periods of tone, whereas values below the threshold were classified as atonia.

A similar procedure was applied to the LFP signal to differentiate high-delta and low-delta periods. Segments of NREM sleep and REM sleep (defined below) were used to establish median amplitudes, and the midpoint between them was taken as the delta threshold.

Periods of high delta power and behavioral quiescence were classified as NREM sleep. Periods of nuchal atonia and low delta power were classified as REM sleep. To avoid spurious state transitions, any putative change in state was required to persist for at least 5 s; otherwise, the animal was considered to have remained in the prior state. Data were analyzed continuously (i.e., not in 5 second bins), allowing bouts to begin at any time, but transient deviations shorter than 5 seconds were ignored. Thus, brief arousals (including postural adjustments and stretching) lasting less than 5 seconds in duration did not end a NREM bout. Periods not classified as NREM or REM sleep were considered wake. Active wake was defined as that part of the wake period that was within 3 s of movement detected by the ROI Movement Classification; all other timepoints were considered quiet wake. This ensured that all quiet wake periods were not overlapped with sleep, and at least 3 s from any movement.

Temporal Analysis of Twitch Rate. To characterize the temporal evolution of twitching within REM sleep, twitch timestamps were aligned to the onset of their respective bouts. For each bout, a continuous estimate of twitch rate was generated using a 2-s sliding window (running mean). These bout-level rates were then calculated for each pup to obtain a representative mean twitch rate trajectory. Finally, these individual trajectories were combined to calculate the grand mean twitch rate for all pups at each age group.

Division of tonic and phasic REM substates. Within REM sleep, periods were further classified as tonic or phasic REM based on the occurrence of myoclonic twitches. Twitch events were identified from the manually scored movements of all body parts (forelimb, hindlimb, whisker, and tail). For each twitch, the window centered on the event (±2 s from twitch onset) was designated as phasic REM, similar to approaches and durations used in previous rodent studies (Burgess et al., 2008; Anaclet et al., 2010; Dong et al., 2022). All remaining periods of REM sleep that did not overlap with any phasic window were classified as tonic REM. This approach ensured that phasic REM encompassed both the twitch itself and any associated oscillatory change preceding or following the movement, while tonic REM reflected periods of muscle atonia and relative motor quiescence.

Power Spectrum Analysis. LFP activity was analyzed across behavioral states, including quiet wake, active wake, REM sleep, and NREM sleep. Power spectral densities were computed in MATLAB using the pspectrum() function with default parameters. The resulting spectra were expressed relative to quiet wake by converting power values to decibel (dB) units. Quiet wake served as the normalization baseline because it occurs alongside behavioral quiescence, removing the possibility of movement artifact, and lacks strong state-dependent rhythmic activity—such as the theta oscillations typical of REM sleep or the delta and sleep spindle activity characteristic of NREM sleep.

Quantification and statistical Analysis

Spike Sorting. Neural recordings acquired in SynapseLite were converted to binary format using custom MATLAB scripts and processed in Kilosort 2.0 (Pachitariu et al., 2016). Prior to spike detection, data were whitened (covariance-standardized) and band-pass filtered between 300 and 5000 Hz. Event waveforms were sorted into clusters through template matching. The initial spike detection threshold was set to six standard deviations below the mean signal, followed by a second-pass threshold of five standard deviations. A minimum firing rate of 0.01 spikes/s was required for inclusion, and the bin size for template estimation was set to 262,400 samples (approximately 11 s). All other Kilosort parameters were maintained at default values.

Cluster visualization and manual curation were performed in Phy2 (Rossant and Harris, 2013). Units were classified as putative single neurons if their spike waveforms consistently conformed to a single template, appeared as distinct, well-isolated clusters in principal component space, and exhibited a clear refractory period in their auto-correlogram (manifested as reduced firing at zero-time lag). Clusters meeting the first two criteria but lacking a refractory period were categorized as multi-units and excluded from further analysis.

Units displaying waveform characteristics suggestive of electrical noise, firing rates below 0.01 spikes/s, or amplitude instability over time were also excluded. To verify unit isolation, cross-correlograms of all single- and multi-unit pairs recorded on neighboring channels were compared. When cross- and auto-correlograms exhibited similar features, clusters were merged and reclassified as multi-units when appropriate.

Statistical Analyses. All statistical analyses were conducted in MATLAB. The significance threshold (α) was set at 0.05 for all tests, and Bonferroni corrections were applied when multiple comparisons were performed. Unless otherwise stated, data are presented as mean ± standard

error of the mean (SEM). Depending on the experimental design, differences were evaluated using a one-way ANOVA, two-way ANOVA, or *t*-tests. If data were not normally distributed, the non-parametric equivalents of these tests were used.

To quantify the temporal trajectory of twitching at the onset of REM sleep, linear regression models were fitted to the mean twitch rate over the first 30 s of REM for each animal using the MATLAB function fitlm(). The slope and y-intercept were extracted from each individual model to serve as dependent variables for subsequent age-group comparisons.

Violin plots were generated with outliers removed, as determined by MATLAB's isoutlier() function. This function identifies and excludes data points that deviate by more than three scaled median absolute deviations from the sample median. The survivor plot of tonic REM bout length was tested for significance using the MatSurv() function for MATLAB with its default parameters (Creed et al., 2020).

Results

To establish the developmental emergence of tonic and phasic REM sleep, we recorded motor and brain activity in unanesthetized rats at P12, P16, P20, and P24. This was a cross-sectional design, as each age cohort consisted of different animals. As described in detail above, rats were tested in the Mobile HomeCage, an air table that allows rat pups to locomote while head-fixed, in a recording environment that was approximately 29° C, which is permissive of REM sleep (Szymusiak and Satinoff, 1981). Together, this allowed us to record significant periods of REM and NREM sleep on the day of surgery. Neurophysiological signals were recorded in the forelimb region of M1 (P12: N = 9 pups; P16: N = 11 pups; P20: N = 12 pups; P24: N = 10 pups; **Figure S1A, B**). Neural activity, electromyographic activity of the nuchal and biceps muscles, and high-speed video (100 frames/s) were recorded continuously for 3-6 h. Recordings were performed entirely during the lights-on period (1000 to 1800 hours).

REM and NREM sleep oscillations from P12 to P24

In rodents, myoclonic twitches of the skeletal muscles often define phasic REM, whereas periods of REM sleep lacking twitches define tonic REM (Vogel et al., 2000; Brankačk et al., 2012; Meng et al., 2021; Dong et al., 2022; Bueno-Junior et al., 2023). Thus, to be inclusive of both tonic and phasic REM, we avoided defining REM based on twitches and instead relied on two electrophysiological criteria. The first criterion was nuchal muscle atonia. Because nuchal atonia may also occur during NREM sleep (Seelke and Blumberg, 2008), the second electrophysiological criterion was low delta power. **Figure 1** shows the mean change in nuchal tone at the onset and offset of REM sleep (**Figure 1A**), along with the decrease in delta power at the onset of REM sleep (**Figure 1B**). Periods of behavioral quiescence and high delta power were classified as NREM sleep. All timepoints not classified as REM or NREM sleep were classified as wake, which we split into periods of quiet wake (lacking movement) or active wake (with movement).

At all ages, rats cycled between NREM sleep, REM sleep, and wake throughout the recording session (**Figure S1C**). The percentage of time spent in REM sleep ($F(3,38) = 35.65$, $p < 0.0001$) and wake ($F(3,38) = 15.84$, $p < 0.0001$) varied significantly by age, while the percentage of time spent in NREM sleep did not ($F(3,38) = 2.51$, $p = 0.073$; **Figure 1C**). Consistent with previous reports (Jouvet-Mounier et al., 1969), younger pups spent significantly more time in REM sleep, with P12 pups spending 34.3 ± 2.8% of overall time in REM sleep, whereas P20 and P24 pups spent 7.4 ± 0.9% and 7.4 ± 1.0%, respectively. This was accompanied by a corresponding increase in the percentage of time spent awake (50.0 ± 4.3% and 78.7 ± 2.5% at P12 and P24, respectively).

Beyond changes in sleep architecture, the spectral composition of the LFP differed markedly between states. **Figure 1D** shows the increased delta power (0.5-4 Hz) of NREM sleep relative to quiet wake. At P16, P20, and P24, NREM sleep in M1 also showed an increase in alpha (8-15 Hz) power, likely reflecting the developmental emergence of sleep spindles, which in humans appear in the first 2 postnatal months (Robert, 1982 p.198; Sokoloff et al., 2021). In contrast, REM sleep at P12 was characterized by a global increase in power across all frequencies compared to quiet wake. At P16, P20, and P24, periods of REM sleep showed an increase in power restricted to the theta band (4-8 Hz), along with a decrease in power in the delta and alpha bands (**Figure 1E**). REM sleep was also associated with an increase in slow gamma power. The developmental emergence of prominent theta power in M1 between P12 and P16 was also evident in the raw power spectrum; increased power in the theta band was not present at P12, but was present at P16, P20, and P24 (**Figure S2**).

Increasing delay from REM onset to first twitch

Representative recordings of the onset of REM sleep at each age are shown in **Figure 2**, illustrating the defining electrophysiological and behavioral features of the state across development. Each panel shows the characteristic drop in nuchal EMG tone and reduction in delta power in the LFP at REM onset. From P16 onward, an approximately 6 Hz theta band oscillation is also visible. Myoclonic twitches were readily observed during REM sleep at all ages, although their temporal distribution within each bout changed markedly with age.

In P12 pups, twitches occurred almost immediately following the onset of REM sleep, often continuing throughout the bout. By contrast, at P20 and P24, the first twitch was delayed, producing an extended period of atonia without twitches—resembling tonic REM in older animals. These representative traces suggest a developmental shift in the structure of REM sleep, from bouts dominated by phasic activity at early ages to longer bouts containing a clear tonic phase preceding clusters of twitches.

To quantify the change in twitch timing across development, every REM bout was plotted as a raster of twitches, ordered by bout duration (**Figure 3A**). Each tick mark represents a scored twitch from any body part. At P12, twitches were distributed relatively uniformly throughout each REM bout, producing a dense, continuous pattern. By P16, however, the onset of each REM bout was often marked by a pause in twitching, followed by a return to regular twitch activity. This trend became more pronounced at P20 and P24, where the early portion of each bout was dominated by extended periods of atonia with little or no twitching, followed by a progressive increase in twitch rate later in the bout. This "ramp-up" pattern is evident in the mean twitch rate (**Figure 3A**, bottom traces). Whereas the P12 rate fluctuates around the overall mean (red dashed line) from the very onset of the bout, older ages exhibit a distinct trajectory: starting closer to zero and rising gradually to meet the mean.

Figure 3B zooms in on the first 30 seconds of REM bouts for each age. To characterize the developmental emergence of the initial "quiet" period, we performed a linear regression on the mean twitch rate for each animal (light blue lines) and the group mean (dark blue line). Whereas the regression still shows a positive slope at P12, this age shows a high y-intercept, indicating that twitching begins immediately in REM bouts. In contrast, the slopes steepen and the intercepts drop in older animals.

We quantified these parameters in **Figures 3C** and **3D**. The y-intercept of the fit line (**Figure 3C**, blue line)—representing the estimated twitch rate at the exact moment of REM onset—decreased significantly with age ($F(3,38) = 19.9$, $p = 0.0002$). Specifically, the intercept showed a significant drop from 0.59 Hz at P12 to 0.15 Hz at P16, reaching a floor of ~0.04–0.08 Hz at P20 and P24. Notably, this drop in the y-intercept was much larger than the mild age-related decline in the overall mean twitch rate (**Figure 3C**, black line). However, unlike the y-intercept, the slope did not significantly vary with age (**Figure 3D**; $F(3,38) = 1.09$, $p = 0.78$), demonstrating that the developmental emergence of this REM without twitching is driven by a suppression of twitching at REM onset rather than a change in the rate at which twitches accumulate over time.

To directly measure the duration of this period of twitchless REM, we calculated the latency from REM onset to the first twitch for every bout (**Figure 3E**). Median latency to the first twitch increased systematically with age from P12 to P20 (P12: 2.1 s; P16: 6.5 s; P20: 12.3 s; P24: 12.0 s). A one-way Kruskal-Wallis test revealed a significant main effect of age on latency to first twitch ($H(3) = 343.3$, $P<0.0001$), with post-hoc comparisons showing significant increases from P12 to P16 and again from P16 to P20. These results confirm a developmental shift in REM sleep architecture from bouts dominated by phasic activity to those containing a distinct tonic phase preceding the onset of twitching.

Developmental differentiation of tonic and phasic REM sleep

To determine whether this developmental difference in the latency to the first twitch captured broader developmental changes in REM sleep structure, REM bouts were subdivided based on the timing of twitches. We focused on myoclonic twitches across the entire body as a global measure of phasic activation. In light of the different developmental trajectories of specific body parts reported previously (Dooley et al., 2021), this approach should provide a more stable index of the phasic REM across this age range compared to choosing a single body part (i.e. whiskers). Accordingly, periods within ±2 s of any behaviorally scored twitch were classified as phasic REM, and all remaining periods of REM sleep were tonic REM (**Figure 4A**).

With increasing age, pups spent a decreasing percentage of time in phasic REM relative to tonic REM (**Figure 4B**). Tonic REM occupied 34.1% of total REM at P12, 47.6% at P16, 53.2% at P20, and 63.6% at P24. A one-way ANOVA revealed a significant effect of age on the percentage of tonic REM ($F(3,38) = 14.8$, $p < 0.0001$). Post-hoc comparisons show a steady increase in tonic REM across age, with each age differing significantly from the preceding age.

We also observed that the overall twitch rate during REM sleep decreased significantly with age (**Figure 4C**; $F(3,38) = 8.00$, $p < 0.0005$), reflecting the overall reduction in phasic activity. However, within phasic REM periods, the twitch rate remained stable across ages ($F(3,38) = 1.32$, $p = 0.28$), indicating that while the overall twitch rate decreased across development, its rate within phasic episodes did not change.

Although tonic REM bouts were distributed relatively uniformly across the REM bout at P12, by P16 they were much more likely to occur at the start of the bout (**Figure 4D**). This tendency for REM bouts to begin in tonic REM strengthened further at P20 and P24, with 80% of bouts starting in tonic REM, mirroring the typical sequence seen in adult rodents (Bueno-Junior et al., 2023; Boscher et al., 2024). We also observed a significant age-related difference in the duration of tonic REM bouts, with bouts being shortest at P12 and longest at P24 (**Figure 4E**; logrank test, $\chi^2 = 475.72$, df = 3, $p < 0.0001$). At P12, only 5.7% of tonic REM bouts were 10 seconds or longer, whereas at P24 this proportion increased to 27.9%.

Neural activity in M1 also differed systematically between tonic and phasic REM (**Figure 4F**). At every age, single-unit firing rates were significantly higher during phasic than tonic REM (P12: $t(8) = -3.9$, $p < 0.005$; P16: $t(10) = -3.62$, $p < 0.005$; P20: $t(11) = -4.76$, $p < 0.0001$; P24: $t(9) = -3.21$, $p < 0.01$), consistent with prior reports in rodents that phasic REM is accompanied by increased cortical activity (McCarley and Hobson, 1970; Bueno-Junior et al., 2023). Together, these findings suggest that by the end of the third postnatal week, REM sleep in rats is differentiated into alternating tonic and phasic substates that resemble those described in adult rodents (Brankačk et al., 2012; Bueno-Junior et al., 2023).

Oscillatory differences between tonic and phasic REM

Spectral analyses of M1 LFPs revealed that tonic and phasic REM differ not only in motor activity but also in their oscillatory composition (**Figure 5**). Relative to quiet wake, phasic REM at P12 was characterized by a broadband increase in power, whereas tonic REM showed a uniform decrease in power below ~20 Hz. This broad increase in power during phasic REM is likely the result of event-related potentials produced by the long duration response to twitches at this age (Dooley and Blumberg, 2018; Reid et al., 2025). Beginning at P16, both tonic and phasic REM exhibited an increase in power at gamma (30-55 Hz) and fast gamma (65-100 Hz) frequencies (**Figures 5A, C**) compared to quiet wake (Brankačk et al., 2012). Phasic REM showed significantly higher power than tonic REM in both gamma bands, consistent with prior reports in humans (Simor et al., 2016; Avigdor et al., 2025) and rodents (Brankačk et al., 2012; **Figure 5C**).

Beginning at P16, a prominent theta peak (4–8 Hz) emerged in both tonic and phasic REM, increasing in strength at each subsequent age. The prominence of this theta band is particularly evident at P20 and P24, where relative to quiet wake the theta peak is accompanied by a dip in power of the frequencies directly above and below theta (**Figure 5B**). To assess whether theta frequency differed between REM substates within each age, we performed paired *t*-tests at P16, P20, and P24 (**Figure S3B**). At P16, theta frequency did not differ significantly between phasic and tonic REM ($t(10) = 0.48$, $p = 0.64$). By P20, theta frequency was significantly higher during phasic REM (6.08 ± 0.08 Hz) than tonic REM (5.80 ± 0.08 Hz; $t(11) = 8.2$, $p < 0.0001$). A similar pattern was present at P24, where phasic REM exhibited faster theta (6.09 ± 0.06 Hz) than tonic REM (5.91 ± 0.07 Hz; $t(9) = 3.00$, $p = 0.015$). Together, these comparisons indicate that reliable substate differences in theta frequency emerge by P20 and are maintained at P24, which is consistent with prior work in adult rodents (Vanderwolf and Robinson, 1981; Bueno-Junior et al., 2023).

Finally, at P24, we found a significant difference between tonic and phasic REM in the alpha band ($t(9) = -3.50$, $p < 0.0001$; **Figure 5C**), illustrating an increase in power in the alpha band during tonic REM. An increase in alpha power during tonic REM was also observed at P20, though not significant ($t(11) = -3.11$, $p = 0.091$). Strikingly, this was the only instance across all ages and frequency bands where power was significantly higher during tonic REM than phasic REM. The emergence of a tonic REM alpha oscillation parallels prior findings in humans (Simor et al., 2016, 2019). Together, these results highlight a developmental trajectory toward the substate-specific oscillatory patterns seen in adults, marking the emergence of distinct tonic and phasic REM dynamics by P24.

Discussion

In adults, REM sleep consists of distinct tonic and phasic substates, each with distinct behavioral and physiological features. Here, we demonstrate that these substates emerge gradually from an early, undifferentiated state. At P12, REM sleep is dominated by twitches, behaviorally resembling phasic REM while lacking distinct oscillatory features. By P16, however, tonic REM begans to appear at the onset of bouts, acquiring specific oscillatory signatures—including an alpha rhythm—by P24. Conversely, phasic REM maintains its characteristic high neural activity and stable twitch rates while developing its own distinct oscillatory features. Thus, as the undifferentiated REM sleep of infancy evolves into the complex REM sleep of adulthood, the emergence of tonic REM may mark a transition toward representational capacities that rely less on moment-to-moment sensorimotor input and more on internally coordinated cortical dynamics.

Increasing complexity of sleep states across development

Sleep in early life is dynamic, reflecting the ongoing development of neural circuits. In the first postnatal week, cortical activity is characterized by intermittent, sensory-driven bursts separated by silence (Khazipov et al., 2004). At this age, pups cycle between wake and REM sleep, defined by muscle atonia punctuated by myoclonic twitches (**Figure 6**). In the second postnatal week, a quiescent sleep state emerges, eventually acquiring the continuous delta oscillations that define NREM sleep by P12 (Blumberg et al., 2005; Seelke and Blumberg, 2008), marking the onset of a stable two-state sleep cycle.

Building on this developmental milestone, our findings demonstrate that REM sleep itself subsequently undergoes a gradual differentiation. Although we identified twitch-free periods of REM sleep in P12 pups, a consistent bout structure—where twitch-free tonic REM reliably initiated the bout—did not stabilize until P16. This behavioral organization is paralleled by the emergence of distinct oscillatory signatures: while phasic REM maintains elevated gamma power and neural firing, tonic REM gradually acquires a distinct fast-alpha oscillation. The proportion of tonic REM also increased across development (from ~34% at P12 to ~64% at P24), which is consistent with previous reports (Vogel et al., 2000), reflecting a continuous transition toward the tonic-dominated architecture of adult REM sleep (Brankačk et al., 2012). Yet despite the growing prevalence of tonic REM, the rate of twitching within phasic episodes remained stable from P12 to P24. This persistence suggests that, even as phasic REM occupies a smaller share of total sleep, its defining behavioral and neural features are preserved—consistent with a conserved role in sensorimotor integration and plasticity across development.

Together, these findings position the emergence of tonic and phasic REM as the latest refinement in a developmental continuum of sleep organization—beginning with the active sleep of neonates and culminating in the complex, layered architecture of the juvenile and adult brain.

Functional roles of phasic and tonic REM

Phasic REM is defined by the appearance of twitches and rapid eye movements that are accompanied by bursts of cortical activity and elevated theta and gamma power. In humans, this coincides with increased arousal thresholds and reduced sensory responsiveness (**Table 1**), indicative of a brain deeply engaged in internally-generated patterns of activity. In contrast, tonic REM is characterized by the absence of movements and increased alpha power—features that more closely resemble relaxed wakefulness. Theta oscillations are slower, cortical activity is lower, and, at least in humans, sensory responsiveness is partially restored, suggesting a partial re-engagement with the external world. REM bouts typically begin in the tonic state before transitioning to a phasic state, reflecting a shift from externally receptive to internally driven modes of processing.

The presence in early infancy of a state that—at least behaviorally—resembles phasic REM strongly supports the idea that these behaviors serve a fundamental developmental function. Myoclonic twitches, the defining feature of phasic REM, are expressed against a backdrop of muscle atonia and generate bursts of sensory feedback that reverberate throughout the somatosensory and motor systems. These twitches provide temporally precise neural activity that in rodents have been shown to help to construct and refine sensorimotor circuits (Blumberg et al., 2022), shape sensory maps (Dooley and Blumberg, 2018; Gómez et al., 2021, 2023), and calibrate internal models of movement (Dooley et al., 2021). As development proceeds, however, REM sleep includes longer and longer periods of twitch-free quiescence—suggesting a distinct, yet complementary, REM sleep substate.

If phasic REM provides the scaffold for building sensorimotor representations, what might be the function of the activity driven by the later-emerging tonic REM? Unlike phasic REM, tonic REM is marked by behavioral quiescence and, in humans, increased sensory responsiveness, driven by the partial re-engagement of thalamocortical sensory pathways (Wehrle et al., 2007). These observations suggest that the two substates promote distinct modes of neural coordination: phasic REM strengthens activity patterns that arise from self-generated movements, whereas tonic REM organizes patterns of activity that occur in the absence of movement—more akin to the sensory attention or contextual processing typical of quiet, reflective wakefulness.

Consistent with this distinction, dream studies in humans report that individuals awakened during phasic REM describe vivid, movement-rich scenes, whereas those awakened during tonic REM describe more static or observational imagery (Berger, 1968; Wehrle et al., 2007). While inherently subjective and limited to humans, these reports provide a framework for linking behavioral quiescence, sensory responsiveness, and network activity. Viewed developmentally, this sequential pattern—phasic REM followed by tonic REM—suggests that linking self-generated movements to sensory feedback may be a prerequisite for later representations of sensory input independent of movement.

In this framework, the emergence of tonic REM in rats around the end of the third postnatal week may represent more than a change in oscillatory patterning—it signals the onset of coordinated cortical activity capable of sustaining internally-generated sensory representations in the absence of movement. Phasic REM continues to provide the building blocks of embodied experience through sensorimotor reactivation, while tonic REM introduces a state in which these newly established circuits can be stabilized, synchronized, and integrated across cortical areas. Together, these complementary modes of REM sleep may provide the foundation for the increasingly complex forms of behavior emerging during the transition from infancy to juvenile life. By parsing REM sleep into its component substates, we can begin to trace how sleep's functions expand in parallel with development.

Limitations and future directions

Several limitations of the present study are worth considering. First, recordings were acutely performed in head-fixed animals. Although all pups readily slept and displayed clear behavioral and electrophysiological signatures of REM and NREM sleep, immobilization likely influenced bout structure, particularly at older ages where REM bouts were often shorter than those described in freely moving rodents (e.g., Boyce et al., 2016; Bueno-Junior et al., 2023). Likewise, although cortical dynamics typically recover within the provided acclimation period (Domínguez et al., 2021), residual anesthetic effects from these acute experiments may still have influenced sleep dynamics.

Second, we did not assess behavioral arousal thresholds, which in adult humans differ between phasic and tonic REM (Stuart and Conduit, 2009; Ermis et al., 2010), offering another potential

difference between these substates. However, to date no rodent studies have measured behavioral arousal thresholds across tonic and phasic REM (**Table 1**). While behavioral data are lacking, cellular mechanisms of sensory gating have been explored in mice: thalamic somatosensory neurons become hyperpolarized during tonic REM, consistent with strong sensory inhibition (Boscher et al., 2024). Conversely, during phasic REM, the membrane potential exhibits wake-like depolarization, suggesting a window of heightened sensory permeability, particularly compared to tonic REM. Although these cellular findings in mice appear contradictory to human behavioral results, they rely on different sensory modalities: human studies have assessed thresholds in the auditory system, whereas rodent findings reflect inhibition in the somatosensory system. The discrepancy may therefore arise from differences between sensory modalities, rather than conflicting conclusions about REM substates.

Third, our analysis relied on categorical thresholds to define tonic and phasic bouts. While this approach effectively captured the broad developmental shift toward tonic REM, it imposes binary boundaries on what may be a physiological continuum. Recent work in adult mice suggests that REM sleep is organized along a gradient of arousal and autonomic activation, with tonic and phasic states representing the poles of this spectrum rather than discrete switches (Bueno-Junior et al., 2023). Consequently, the developmental "expansion" of tonic REM described here might reflect a shift in the probability distribution of this continuum towards the tonic pole. Future analyses—moving beyond categorical percentages and instead focusing on dynamic, continuous metrics—may better characterize the developmental differences identified here.

Altogether, these constraints highlight important next steps. The present results provide a foundation for future studies using freely moving preparations and physiological measures of arousal using multiple modalities to more fully characterize how REM sleep and its substates change across early development and into adulthood. Such approaches will be critical for linking behavioral state transitions to their underlying neural dynamics and for testing how substate organization contributes to the emergence of sleep–wake architecture.

References

Anaclet C, Pedersen NP, Fuller PM, Lu J (2010) Brainstem Circuitry Regulating Phasic Activation of Trigeminal Motoneurons during REM Sleep. PLOS ONE 5:e8788.

Avigdor T, Peter-Derex L, Ho A, Schiller K, Wang Y, Abdallah C, Delaire E, Jaber K, Travnicek V, Grova C, Frauscher B (2025) Spectral and network investigation reveals distinct power and connectivity patterns between phasic and tonic REM sleep. Sleep 48:zsaf133.

Berger RJ (1968) Characteristics of Rem Sleep following Different Conditioned Rates of Waking Eye Movement in the Monkey. Percept Mot Skills 27:99–117.

Blumberg MS, Dooley JC, Tiriac A (2022) Sleep, plasticity, and sensory neurodevelopment. Neuron 110:3230–3242.

Blumberg MS, Seelke AMH, Lowen SB, Karlsson KÆ (2005) Dynamics of sleep-wake cyclicity in developing rats. Proceedings of the National Academy of Sciences 102:14860–14864.

Boscher F, Jumel K, Dvořáková T, Gentet LJ, Urbain N (2024) Thalamocortical Dynamics during Rapid Eye Movement Sleep in the Mouse Somatosensory Pathway. J Neurosci 44 Available at: https://www.jneurosci.org/content/44/25/e0158242024 [Accessed January 3, 2025].

Boyce R, Glasgow SD, Williams S, Adamantidis A (2016) Causal evidence for the role of REM sleep theta rhythm in contextual memory consolidation. Science 352:812–816.

Brankačk J, Scheffzük C, Kukushka VI, Vyssotski AL, Tort ABL, Draguhn A (2012) Distinct features of fast oscillations in phasic and tonic rapid eye movement sleep. J Sleep Res 21:630–633.

Bueno-Junior LS, Ruckstuhl MS, Lim MM, Watson BO (2023) The temporal structure of REM sleep shows minute-scale fluctuations across brain and body in mice and humans. Proc Natl Acad Sci USA 120:e2213438120.

Burgess C, Lai D, Siegel J, Peever J (2008) An Endogenous Glutamatergic Drive onto Somatic Motoneurons Contributes to the Stereotypical Pattern of Muscle Tone across the Sleep–Wake Cycle. J Neurosci 28:4649–4660.

Creed JH, Gerke TA, Berglund AE (2020) MatSurv: Survival analysis and visualization in MATLAB. Journal of Open Source Software 5:1830.

Datta S, O'Malley MW (2013) Fear Extinction Memory Consolidation Requires Potentiation of Pontine-Wave Activity during REM Sleep. J Neurosci 33:4561–4569.

De Carli F, Proserpio P, Morrone E, Sartori I, Ferrara M, Gibbs SA, De Gennaro L, Lo Russo G, Nobili L (2016) Activation of the motor cortex during phasic rapid eye movement sleep. Annals of Neurology 79:326–330.

Del Rio-Bermudez C, Kim J, Sokoloff G, Blumberg MS (2017) Theta Oscillations during Active Sleep Synchronize the Developing Rubro-Hippocampal Sensorimotor Network. Curr Biol 27:1413-1424.e4.

668 Domínguez S, Ma L, Yu H, Pouchelon G, Mayer C, Spyropoulos GD, Cea C, Buzsáki G, Fishell
669 G, Khodagholy D, Gelinas JN (2021) A transient postnatal quiescent period precedes
670 emergence of mature cortical dynamics Nelson SB, Moore T, Nelson SB, Colonnese
671 MT, eds. eLife 10:e69011.

672 Dong Y, Li J, Zhou M, Du Y, Liu D (2022) Cortical regulation of two-stage rapid eye movement
673 sleep. Nat Neurosci 25:1675–1682.

674 Dooley JC, Blumberg MS (2018) Developmental “awakening” of primary motor cortex to the
675 sensory consequences of movement. eLife 7.

676 Dooley JC, Glanz RM, Sokoloff G, Blumberg MS (2020) Self-Generated Whisker Movements
677 Drive State-Dependent Sensory Input to Developing Barrel Cortex. Curr Biol 30:2404-
678 2410.e4.

679 Dooley JC, Sokoloff G, Blumberg MS (2021) Movements during sleep reveal the developmental
680 emergence of a cerebellar-dependent internal model in motor thalamus. Curr Biol.

681 Ermis U, Krakow K, Voss U (2010) Arousal thresholds during human tonic and phasic REM
682 sleep. Journal of Sleep Research 19:400–406.

683 Frauscher B, von Ellenrieder N, Dubeau F, Gotman J (2016) EEG desynchronization during
684 phasic REM sleep suppresses interictal epileptic activity in humans. Epilepsia 57:879–
685 888.

686 Gómez LJ, Dooley JC, Blumberg MS (2023) Activity in developing prefrontal cortex is shaped by
687 sleep and sensory experience. eLife.

688 Gómez LJ, Dooley JC, Sokoloff G, Blumberg MS (2021) Parallel and Serial Sensory Processing
689 in Developing Primary Somatosensory and Motor Cortex. J Neurosci 41:3418–3431.

690 Gross DW, Gotman J (1999) Correlation of high-frequency oscillations with the sleep–wake
691 cycle and cognitive activity in humans. Neuroscience 94:1005–1018.

692 Jouny C, Chapotot F, Merica H (2000) EEG spectral activity during paradoxical sleep: further
693 evidence for cognitive processing. NeuroReport 11:3667.

694 Jouvet-Mounier D, Astic L, Lacote D (1969) Ontogenesis of the states of sleep in rat, cat, and
695 guinea pig during the first postnatal month. Developmental Psychobiology 2:216–239.

696 Khazipov R, Sirota A, Leinekugel X, Holmes GL, Ben-Ari Y, Buzsáki G (2004) Early motor
697 activity drives spindle bursts in the developing somatosensory cortex. Nature 432:758–
698 761.

699 Knoop MS, de Groot ER, Dudink J (2021) Current ideas about the roles of rapid eye movement
700 and non–rapid eye movement sleep in brain development. Acta Paediatrica 110:36–44.

701 Koroma M, Lacaux C, Andrillon T, Legendre G, Léger D, Kouider S (2020) Sleepers Selectively
702 Suppress Informative Inputs during Rapid Eye Movements. Current Biology 30:2411-
703 2417.e3.

McCarley RW, Hobson JA (1970) Cortical Unit Activity in Desynchronized Sleep. Science 167:901–903.

Meng Q, Tan X, Jiang C, Xiong Y, Yan B, Zhang J (2021) Tracking Eye Movements During Sleep in Mice. Front Neurosci 15 Available at: https://www.frontiersin.org/journals/neuroscience/articles/10.3389/fnins.2021.616760/full [Accessed November 10, 2025].

Muessig L, Lasek M, Varsavsky I, Cacucci F, Wills TJ (2019) Coordinated Emergence of Hippocampal Replay and Theta Sequences during Post-natal Development. Current Biology 29:834-840.e4.

Nishida M, Uchida S, Hirai N, Miwakeichi F, Maehara T, Kawai K, Shimizu H, Kato S (2005) High frequency activities in the human orbitofrontal cortex in sleep–wake cycle. Neuroscience Letters 379:110–115.

Pachitariu M, Steinmetz N, Kadir S, Carandini M, Kenneth D. H (2016) Kilosort: realtime spike-sorting for extracellular electrophysiology with hundreds of channels. bioRxiv:061481.

Price LJ, Kremen I (1980) Variations in Behavioral Response Threshold Within the REM Period of Human Sleep. Psychophysiology 17:133–140.

Reid MR, Sattler NJ, Dooley JC (2025) Subcortically generated movements activate motor cortex during sleep and wake in rats through postnatal day 24. :2025.01.26.634890 Available at: https://www.biorxiv.org/content/10.1101/2025.01.26.634890v3 [Accessed July 1, 2025].

Robert JE (1982) Development of Sleep Spindle Bursts During the First Year of Life. Sleep 5:39–46.

Rossant C, Harris KD (2013) Hardware-accelerated interactive data visualization for neuroscience in Python. Front Neuroinform 7:36.

Sallinen M, Kaartinen J, Lyytinen H (1996) Processing of auditory stimuli during tonic and phasic periods of REM sleep as revealed by event-related brain potentials. Journal of Sleep Research 5:220–228.

Seelke AM, Blumberg MS (2008) The microstructure of active and quiet sleep as cortical delta activity emerges in infant rats. Sleep 31:691–699.

Seelke AM, Dooley JC, Krubitzer LA (2012) The emergence of somatotopic maps of the body in S1 in rats: the correspondence between functional and anatomical organization. PloS one 7.

Simor P, Gombos F, Blaskovich B, Bódizs R (2017) Long-range alpha and beta and short-range gamma EEG synchronization distinguishes phasic and tonic REM periods. Sleep 41.

Simor P, Gombos F, Szakadát S, Sándor P, Bódizs R (2016) EEG spectral power in phasic and tonic REM sleep: different patterns in young adults and children. Journal of Sleep Research 25:269–277.

741 Simor P, Van Der Wijk G, Gombos F, Kovács I (2019) The paradox of rapid eye movement
742 sleep in the light of oscillatory activity and cortical synchronization during phasic and
743 tonic microstates. NeuroImage 202:116066.

744 Simor P, van der Wijk G, Nobili L, Peigneux P (2020) The microstructure of REM sleep: Why
745 phasic and tonic? Sleep Medicine Reviews 52:101305.

746 Sokoloff G, Dooley JC, Glanz RM, Wen RY, Hickerson MM, Evans LG, Laughlin HM, Apfelbaum
747 KS, Blumberg MS (2021) Twitches emerge postnatally during quiet sleep in human
748 infants and are synchronized with sleep spindles. Current biology 31:3426–3432.

749 Sokoloff G, Uitermarkt BD, Blumberg MS (2015) REM sleep twitches rouse nascent cerebellar
750 circuits: Implications for sensorimotor development. Dev Neurobiol 75:1140–1153.

751 Stuart K, Conduit R (2009) Auditory Inhibition of Rapid Eye Movements and Dream Recall from
752 REM Sleep. Sleep 32:399–408.

753 Szymusiak R, Satinoff E (1981) Maximal REM sleep time defines a narrower thermoneutral
754 zone than does minimal metabolic rate. Physiology & Behavior 26:687–690.

755 Takahara M, Nittono H, Hori T (2002) Comparison of the event-related potentials between tonic
756 and phasic periods of rapid eye movement sleep. Psychiatry and Clinical Neurosciences
757 56:257–258.

758 Takahara M, Nittono H, Hori T (2006) Effect of Voluntary Attention on Auditory Processing
759 During REM Sleep. Sleep 29:975–982.

760 Vanderwolf CH, Robinson TE (1981) Reticulo-cortical activity and behavior: A critique of the
761 arousal theory and a new synthesis. Behavioral and Brain Sciences 4:459–476.

762 Vogel GW, Feng P, Kinney GG (2000) Ontogeny of REM sleep in rats: possible implications for
763 endogenous depression. Physiology & Behavior 68:453–461.

764 Waterman D, Elton M, Hofman W, Woestenburg JC, Kok A (1993) EEG spectral power analysis
765 of phasic and tonic REM sleep In young and older male subjects. Journal of Sleep
766 Research 2:21–27.

767 Wehrle R, Kaufmann C, Wetter TC, Holsboer F, Auer DP, Pollmächer T, Czisch M (2007)
768 Functional microstates within human REM sleep: first evidence from fMRI of a
769 thalamocortical network specific for phasic REM periods. European Journal of
770 Neuroscience 25:863–871.

771 Whitehead K, Slobodina M, Meek J, Fabrizi L (2019) Fronto-central slow cortical activity is
772 attenuated during phasic events in rapid eye movement sleep at full-term birth. Early
773 Human Development 136:45–48.

774

775

Figure 1. Changes in nuchal EMG and delta power at the onset and offset of REM sleep across development.

A Rectified nuchal EMG across all bouts from all animals, aligned to the start and end of each REM bout. Each trace shows mean ± SEM from all bouts. Blue shading indicates the REM period, with time 0 marking the transition into/out of a bout.

B Same as **A**, but for rectified, delta-filtered (0.5–4 Hz) LFP aligned to REM onset, again showing the mean value (± SEM) across all bouts from all animals.

C Mean percentage of time (± SEM) that all animals spent in REM sleep (blue), NREM sleep (green), and wake (red). The percentage of REM sleep decreased in older pups, accompanied by an increase in the amount of time spent in wake. We did not observe a significant difference in the percentage of time spent in NREM sleep. Asterisk denotes a significant difference between subsequent ages when a significant ANOVA was found. Also see **Figure S1,** detailing the sleep-wake architecture of 5 representative animals per age for the entire session.

D Mean decibel-converted LFP power spectra (0.1 to 20 Hz) from M1 during NREM sleep at P12, P16, P20, and P24. For each age, spectra were normalized to power during quiet wake and then the mean was taken across all animals. The colored line represents the mean power for that age and behavioral state, whereas the gray background lines show the corresponding spectra for the other three ages. Frequency bands corresponding to delta (δ) are indicated.

E Same as **D**, but for REM sleep, with the theta (θ) band indicated. For raw (non-normalized) power spectra, see **Figure S2**.

Figure 2. Developmental increase in latency to first twitch at the onset of REM sleep.

200-s segments from P12, P16, P20, and P24 rats illustrating transitions from NREM to REM sleep. For each age, the following signals are shown (top to bottom): scored behavioral state, scored movements (wake movements, arousals, and twitches), ROI-based video analysis of movement, nuchal EMG, M1 LFP trace, M1 LFP spectrogram (0–20 Hz), single-unit spiking activity, and mean spiking activity, calculated over a rolling 250 ms window. Blue shading shows interval from REM onset to the first behaviorally scored twitch at each age. RFL, right forelimb; RHL, right hindlimb; LFP, local field potential.

Figure 3. Developmental emergence of a twitch-free period at the onset of REM sleep bouts.

A Raster plots show the temporal distribution of twitches across the first 150 s of all REM sleep bouts at P12, P16, P20, and P24. Bouts are sorted by duration from longest to shortest. The shaded gray region represents the duration of each bout, and colored ticks indicate individual twitches (RFL, right forelimb; RHL, right hindlimb). The trace below shows the mean twitch rate (black) relative to the overall mean rate for that age (red dashed line).

B Expansion of the first 30 s of the data in **A**. Linear regression models were fitted to the mean twitch rate for each animal (light blue lines) and the group average (dark blue line). The red dashed line indicates the overall mean twitch rate.

C Mean (±SEM) y-intercept derived from the linear fits in **B** (blue), plotted alongside the overall mean twitch rate for each age (black). The blue asterisk denotes a significant difference ($p < 0.05$) in the y-intercept between ages.

D Same as **C** but for the slope of the linear fits.

E Violin plots (log scale) showing the latency from REM onset to the first twitch for all bouts. The asterisk denotes a significant difference ($p < 0.0125$) between ages.

Figure 4. Developmental emergence of tonic and phasic REM sleep.
A Illustration of the criteria used to distinguish tonic and phasic REM sleep. Phasic REM was defined as any REM period occurring within ±2 s of a behaviorally scored twitch; all remaining REM periods were classified as tonic REM.
B Mean percentage (±SEM) of total REM sleep classified as tonic REM for all pups across all ages, with dots indicating the percentage for each pup. Asterisks indicate a significant difference ($p < 0.0125$) between ages.
C Mean twitch rate (±SEM) during all REM (left) and phasic REM (right) for all pups across all ages; gray dots represent individual animals. Asterisks denote significant age differences as in **B**.
D Likelihood of being in tonic (light blue) or phasic (blue) REM for each second of a REM bout (0–150 s). At P12, the likelihood is relatively stable, whereas by P16—and especially by P20 and P24—tonic REM dominates early in the bout before progressively decreasing.
E Survivor plot showing the percentage of tonic REM bouts (y-axis) exceeding the duration on the x-axis (plotted on a semi-log scale). Older pups show a higher percentage of longer-duration tonic REM bouts, indicating more sustained tonic REM sleep.
F Mean M1 spiking rate (spikes/s) during tonic and phasic REM for all animals at all ages. Gray bars denote individual animal means, with the left and right sides of the bar showing the spike rate during tonic and phasic REM, respectively. Black bars denote the overall mean spiking rate across animals at that age. At all ages, M1 neurons fire at a significantly higher rate during phasic REM than during tonic REM ($p < 0.0125$).

Figure 5. Spectral properties of tonic and phasic REM sleep across development.
A, B Decibel-converted mean LFP power spectra from M1 during REM sleep (gray), tonic REM (light blue), and phasic REM (dark blue) for all pups from P12 to P24. As in **Figure 2**, power was normalized to quiet wake. Power is shown from 0.1–100 Hz, with a magnified view of 0.1–12 Hz in **B**. Frequency bands used for beta (12–30 Hz), gamma (30–55 Hz), and fast gamma (65–100 Hz) are indicated. The 55–65 Hz range (notch filter) was excluded from analysis. Raw power data can be found in **Figure S3A.**
B Same as in **A**, magnified to show 0.1–12 Hz. Frequency bands used for delta (0.5–4 Hz), theta (4–8 Hz), and alpha (8–12 Hz) are indicated.
C Mean power (±SEM) for each frequency band during tonic and phasic REM at each age. Data from individual animals are shown as dark blue (phasic, left) and light blue (tonic, right) dots. A dark blue asterisk indicates that phasic REM power significantly differs from 0 ($p < 0.0083$), a light blue asterisk indicates that tonic REM power significantly differs from 0 ($p < 0.0083$), and a black asterisk indicates a significant difference between tonic and phasic REM ($p < 0.0083$).

Figure 6. Developmental progression of sleep state organization.
Schematic summary illustrating the development of the behavioral and neural features of sleep from ≤P9 through P24 and beyond. From left to right, panels depict characteristic features of each state at representative ages, including muscle tone, limb movements, and cortical oscillations (delta, theta, and alpha bands). At ≤P9, sleep consists primarily of wake and active (REM) sleep, with early signs of NREM-like activity emerging at the beginning of sleep bouts. By P12, cortical delta clearly delineates NREM sleep. At P16, the delayed onset of the first twitch following REM onset marks the behavioral emergence of tonic REM, though without any distinct cortical oscillations between tonic and phasic REM. By P24, tonic and phasic REM are fully differentiated, distinguished by their theta frequency, alpha power, twitch rate, and neural activity profiles. Asterisks denote ages at which some—but not all—features of a given state are present.

874
875

Table 1

Citation	*Species*	*Dev. Age*	*Sensory Thresh.*	*Delta 1-4 Hz*	*Theta 4-8 Hz*	*Alpha/Beta 8-30 Hz*	*Gamma 30-200 Hz*	*Notes*
(Sallinen et al., 1996)	Human	Adult	ERP					
(Takahara et al., 2006)	Human	Adult	ERP					
(Wehrle et al., 2007)	Human	Adult	BOLD					
(Price & Kremen, 1980)	Human	Adult	Behav.					
(Takahara et al., 2002)	Human	Adult	ERP					
(Koroma et al., 2020)	Human	Adult	ERP					
(Stuart & Conduit, 2009)	Human	Adult	Behav.					
(Ermis et al., 2010)	Human	Adult	Behav.	X	X	X	X	
(Avigdor et al., 2025)	Human	Adult	-	X	X		X	
(De Carli et al., 2016)	Human	Adult	-			X		
(Waterman et al., 1993)	Human	Adult	-			X		
(Frauscher et al., 2016)	Human	Adult	-	X	X	X		
(Jouny et al., 2000)	Human	Adult	-	X	X	X	X	
(Nishida et al., 2005)	Human	Adult	-			X	+	
(Gross & Gotman, 1999)	Human	Adult	-			+	X	
(Simor et al., 2019)	Human	Adult	-	X*		X	X	*3-4 Hz
(Whitehead et al., 2019)	Human	Neonates	-	X	X			
(Simor et al., 2016)	Human	4-8 years	-	X	X	X	X	
(Boscher et al., 2024)‡	Mouse	Adult	†	X*		X		*2-6 Hz
(Brankačk et al., 2012)	Mouse	Adult	-		X		X	
(Meng et al., 2021)	Mouse	Adult	-		X	X		
(Dong et al., 2022)‡	Mouse	Adult	-		X			
(Bueno-Junior et al., 2023)	Mouse	Adult	-		X	X		

Table 1. Summary of reported differences between tonic and phasic REM sleep in human and mouse studies. This table compiles published comparisons of tonic versus phasic REM across species, highlighting differences in arousal threshold and oscillatory activity. Arousal threshold differences were assessed using auditory stimuli and are indicated by the method used: **ERP** (event-related potentials), **BOLD** (fMRI blood-oxygen-level–dependent responses), or **Behav**. (behavioral measures such as awakening or suppression of eye movements). For each frequency band, an X denotes a significant difference between substates, a + denotes a trend or partial effect, and blank cells indicate no reported difference. Asterisks mark cases where the analyzed frequency band deviated notably from the canonical ranges listed in the header (except for gamma, which commonly represents a narrower sub-range within the broader 30–200 Hz band). A dash (-) indicates that arousal threshold was not tested.

†Substate sensory threshold data could be inferred indirectly from patch-clamp data but were not explicitly quantified.

‡These authors described the two REM substates as “REM with whisking” and “REM without whisking,” which correspond to phasic- and tonic-like periods, respectively.

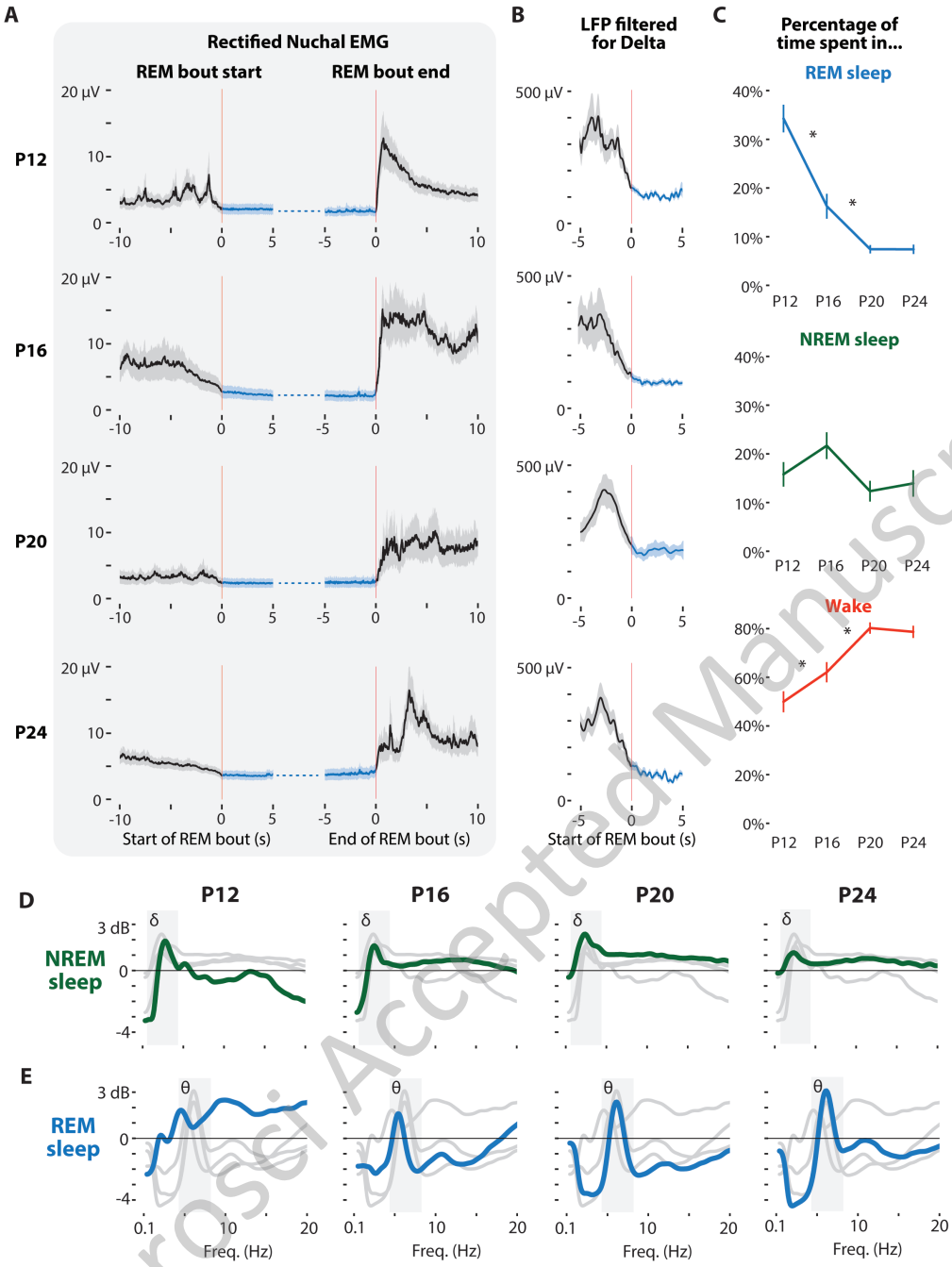

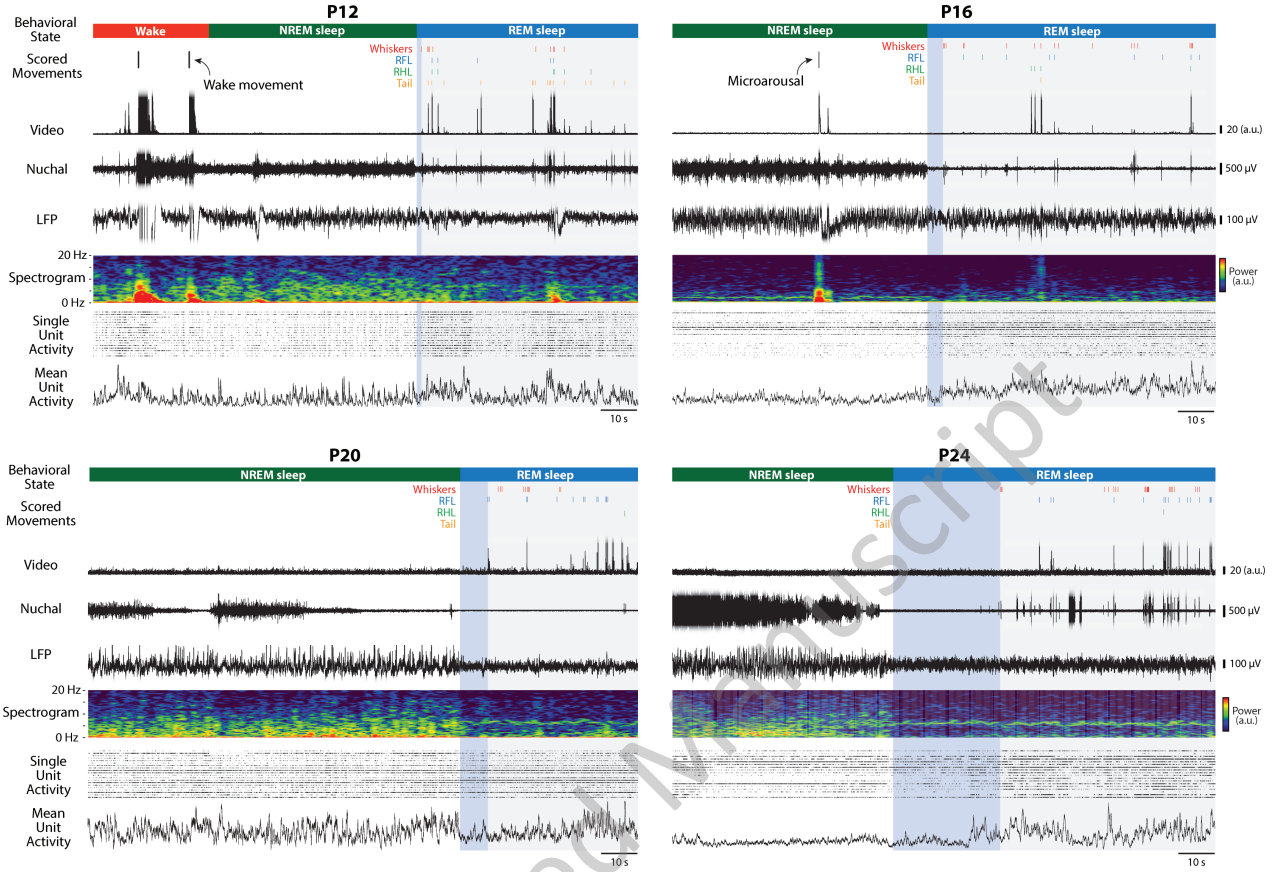

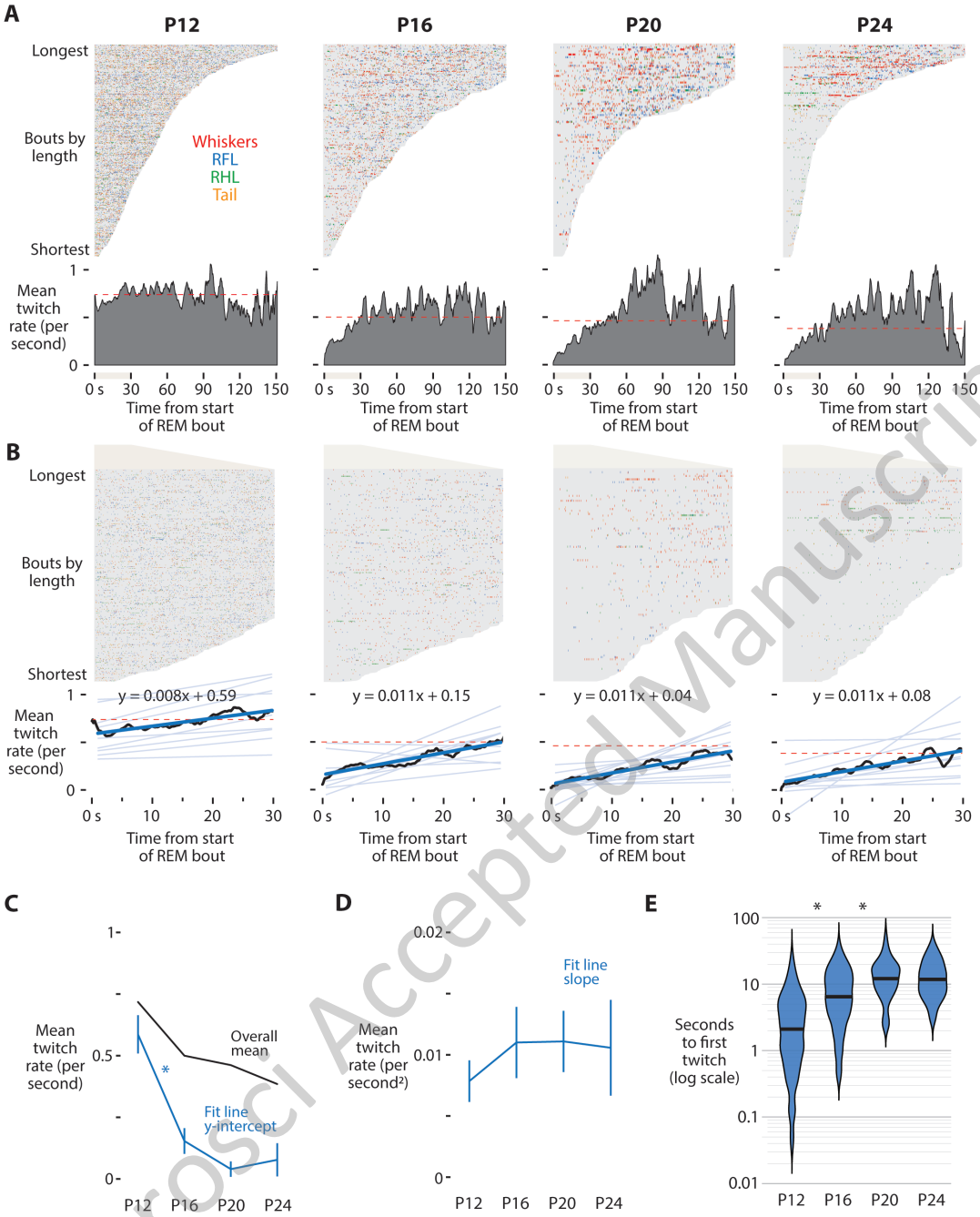

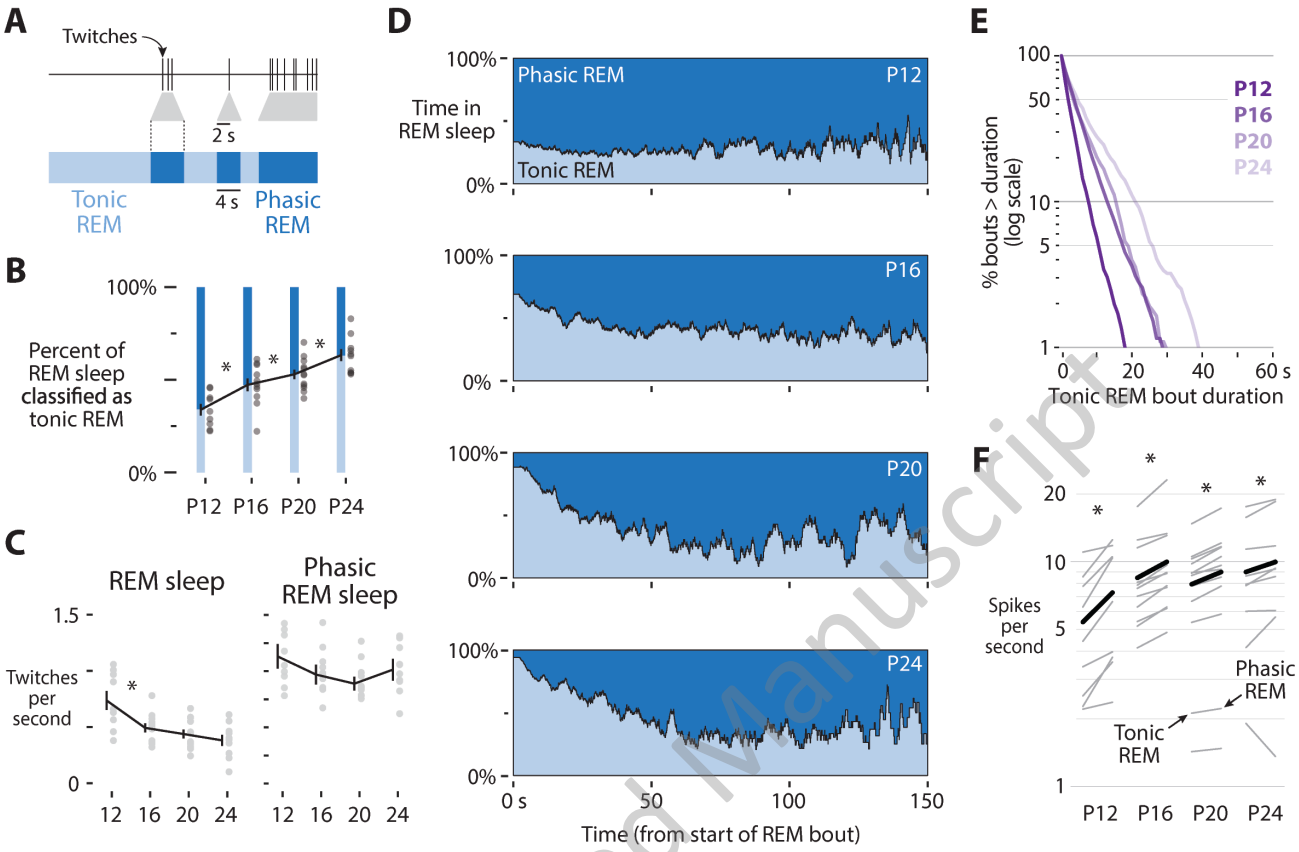

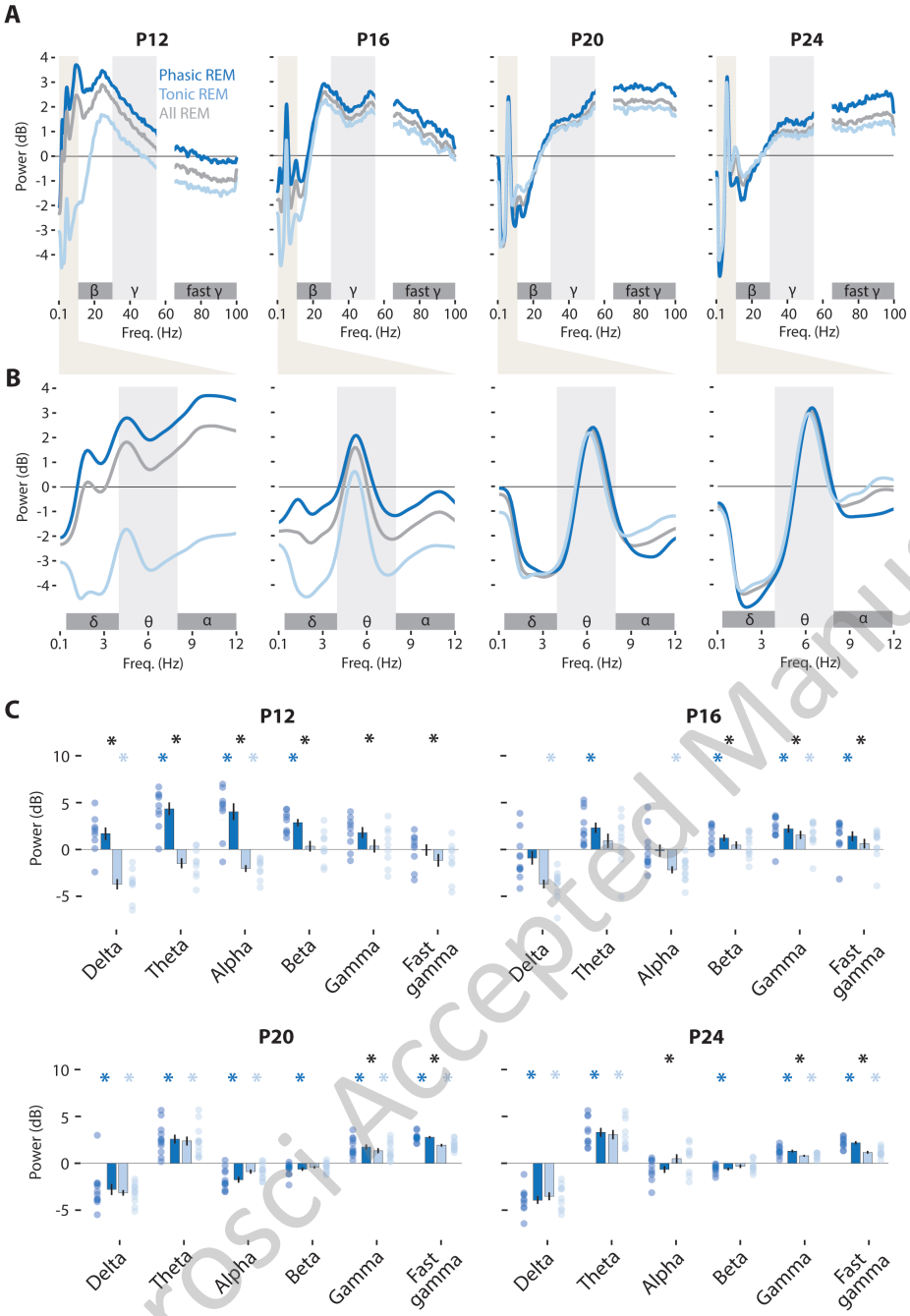

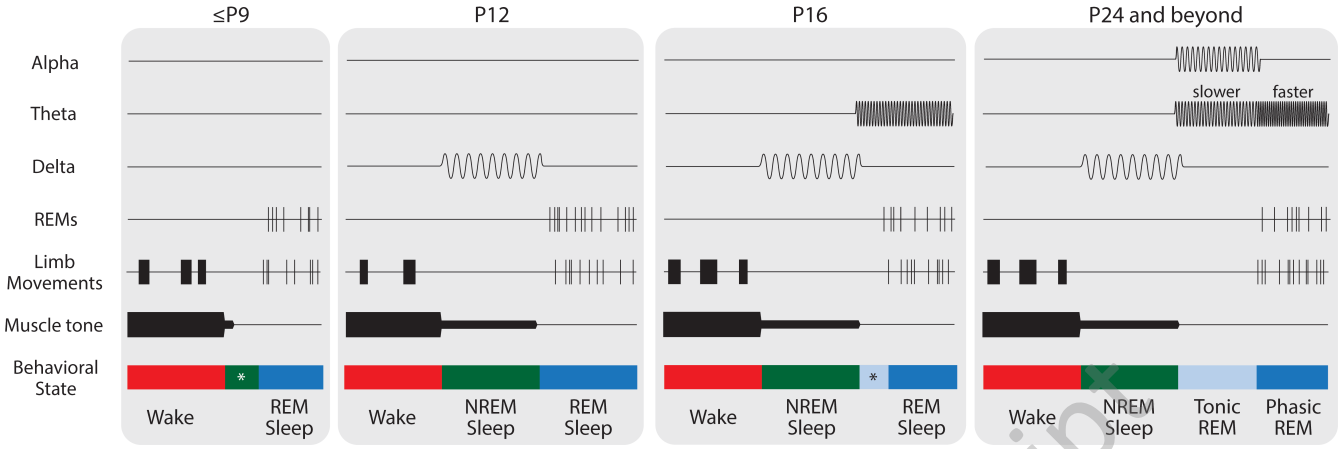

JNeurosci
THE JOURNAL OF NEUROSCIENCE

Supplemental Material

Research Articles | Development/Plasticity/Repair

The developmental emergence of tonic and phasic REM sleep in rats

https://doi.org/10.1523/JNEUROSCI.2176-25.2026

Received: 26 November 2025
Revised: 9 March 2026
Accepted: 12 March 2026

Figure S1

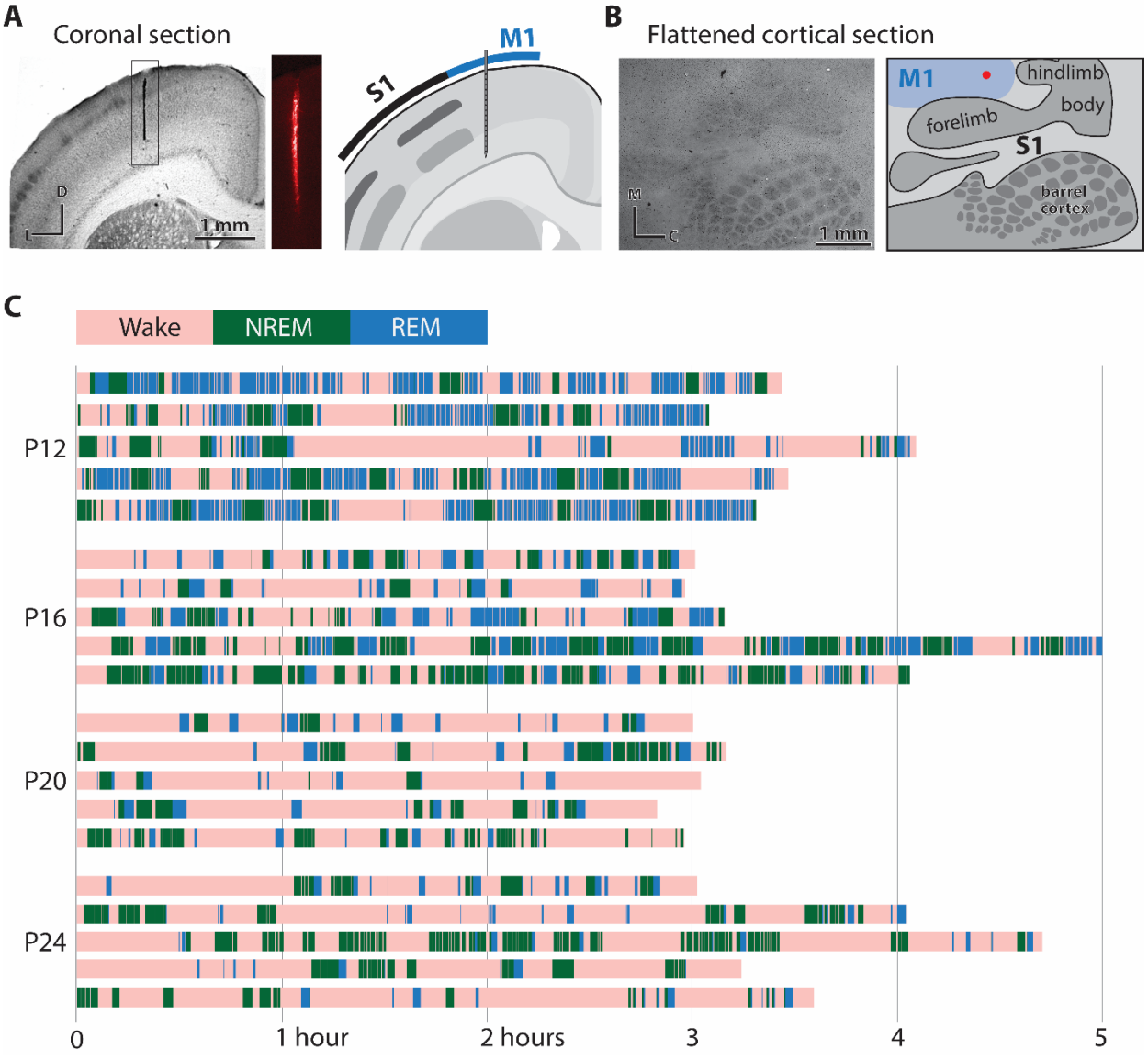

Figure S1. Representative histology and sleep–wake architecture.
A Representative coronal section stained for cytochrome oxidase showing the DiI-labeled electrode track in M1. Borders of primary somatosensory cortex are shown in gray. The black rectangle shows the location of the fluorescent inset to the right, illustrating the DiI-labeled electrode track. Illustration on the right shows the approximate location of the 16 electrode channels.
B Representative flattened cortical section stained for cytochrome oxidase showing the DiI-labeled electrode track in M1 (red dot). Conventions as in **B**.
C Scored behavioral state from 5 representative animals at each age (P12, P16, P20, P24) showing the sequence of behavioral states across the entire recording period. Each row corresponds to a single animal. Behavioral states are color-coded: wake (light red), NREM sleep (green), and REM sleep (blue). The x-axis represents time in hours.

Figure S2

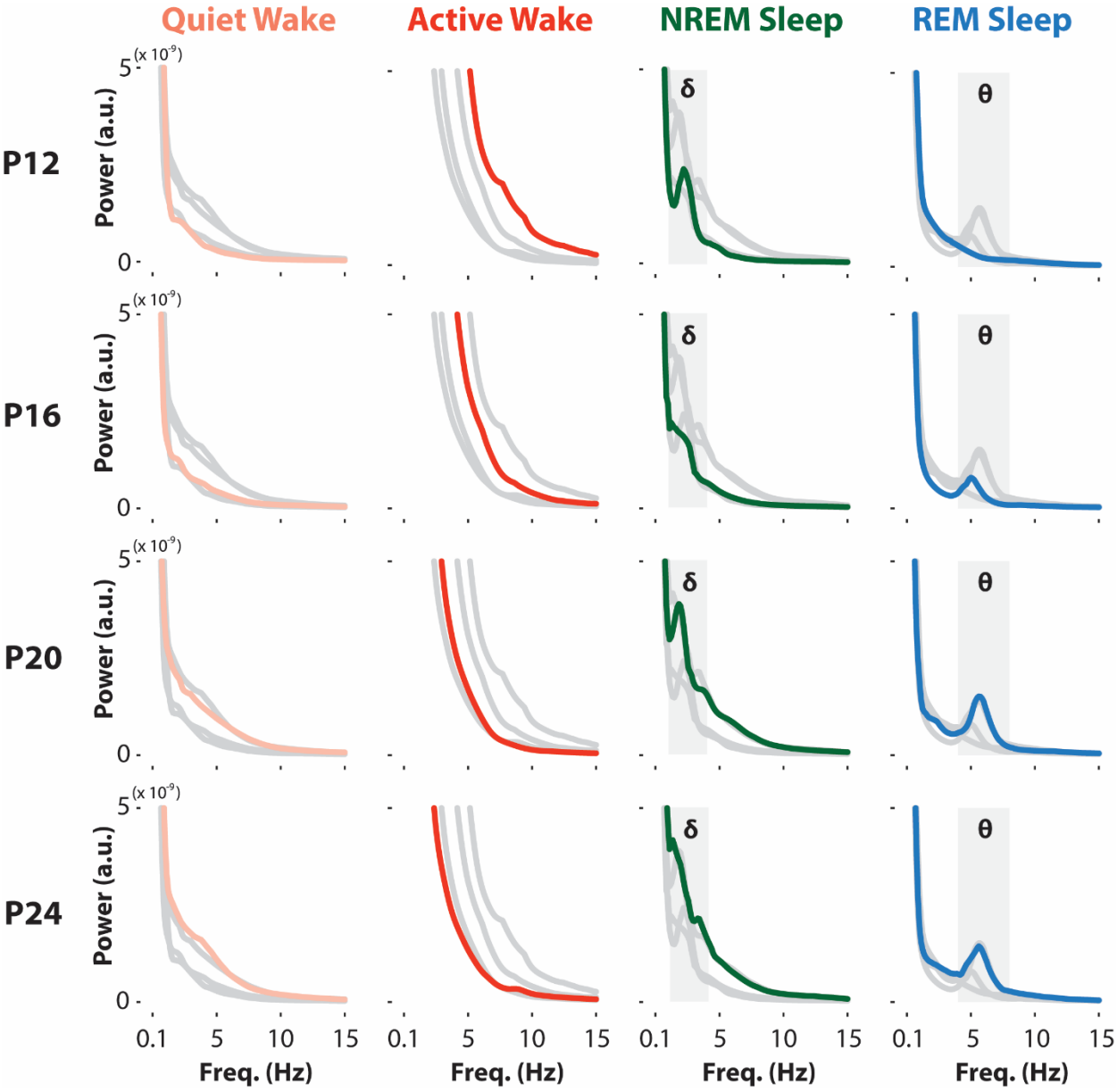

Figure S2 Raw power spectrum across behavioral states across development
Mean raw power spectra (0.1–15 Hz) for all animals across each age (P12 at the top, P24 at the bottom) and each of the four behavioral states (quiet wake, active wake, NREM sleep, REM sleep, from left to right). In each panel, the focal age and behavioral state are shown in color (consistent with the color scheme used in the main text), whereas data from other ages in the same behavioral state are shown in gray. Note the peak in the delta range (1–4 Hz) during NREM sleep and the growing peak in the theta range (4–8 Hz) during REM sleep from P16 onwards.

Figure S3

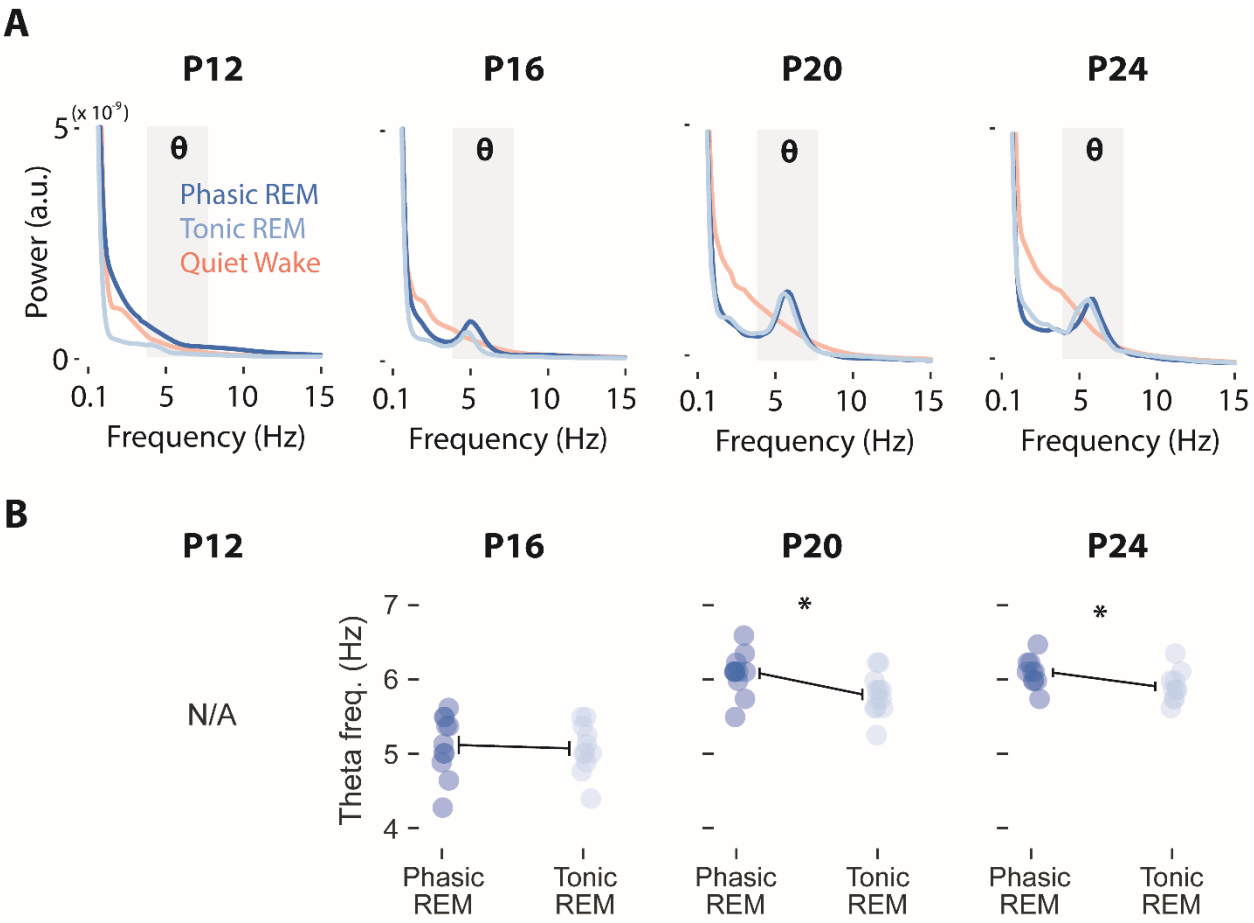

Figure S3. Spectral features of tonic and phasic REM sleep across development. **A** Raw power spectra (0.1–15 Hz) for phasic REM (dark blue), tonic REM (light blue), and quiet wake (light red) at each age (P12, P16, P20, and P24; left to right). **B** Peak theta frequency (Hz) for phasic and tonic REM at each age (P16, P20, P24). Because a peak in the theta band was not present at P12, that age is omitted (see panel **A** and **Figure 5B**). Within each age, paired *t*-tests assessed differences between phasic and tonic REM. Asterisk indicates a significant difference ($p < 0.0125$). Theta frequency did not differ between substates at P16, but was significantly higher during phasic REM at both P20 and P24.